JOURNAL OF MATERIALS SCIENCE 27 (1992) 5306–5314

# The effect of surface constraint on the phase transformation of Nitinol

A. HEDAYAT*, J. RECHTIEN‡, K. MUKHERJEE§
*Department of Metallurgy, Mechanics, and Materials Science, and also ‡Department of Biomechanics, College of Osteopathic Medicine, and §Composite Materials and Structures Center, Michigan State University, East Lansing, MI 48824, USA*

Ultra-low-temperature isotropic carbon was vapour deposited on a near equiatomic Ti–Ni (Nitinol) alloy (49.9 at % Ti–50.1 at % Ni) for components used in biomedical applications. The adhering carbon film, and carbide layer formed after annealing, introduced a surface constraint. Differential scanning calorimetry studies show a marked decrease in the $A_s$ and $M_f$ temperatures of such a surface-constrained alloy during phase transformation. TEM foils made of vertical and horizontal sections of carbon-coated Nitinol were examined using transmission electron microscopy. It is proposed that for surface-constrained samples, the martensite plates last to form were close to the surface, and these are first to disappear during reverse transformation. Moreover, for both coated and uncoated samples, the martensitic and reverse transformations can be described by equations of the form $f(A) = \exp[-\alpha(M_s - T)]$ and $f(A) = \exp[-\gamma(A_f - T)]$, respectively, where $f(A)$ is the fraction of austenitic phase present at the specific temperature ($T$), and $\alpha$ and $\gamma$ are constants. Finally, the driving force for the martensitic and reverse transformations of both coated and uncoated samples was calculated.

## 1. Introduction

The near-equiatomic nickel–titanium alloy (Nitinol) is one that exhibits the shape-memory effect. This is a characteristic by which the alloy can change its shape repeatedly, reversibly, and substantially with heating and cooling [1].

The solid-state martensitic phase transformation in Nitinol (and other such shape-memory alloys) is categorized as being athermal. This type of transformation is a function of temperature and not time. The reaction proceeds only with the change in temperature. If the temperature is held constant, the transformation will not proceed with time.

Thermodynamic studies show that during phase transformation of shape-memory alloys such as Nitinol, the chemical free energy between the parent phase and the martensitic phase is in balance at all times with non-chemical energy, such as elastic energy and surface energy [2, 3]. Because the interface between the martensite and the parent phase is nearly coherent, in a thermoelastic transformation, the surface energy is small. Thus, the opposing non-chemical energy is mainly the elastic energy. The energy relationship of the phase transformation from the parent phase to the martensitic phase, or vice versa, can be represented by the following equation

$$\Delta G = \Delta G_c + \Delta G_{nc} \quad (1)$$

where $\Delta G_c$ is the chemical free energy or driving energy and $\Delta G_{nc}$ is the non-chemical energy [3].

For a first-order phase transformation, a parent phase is in equilibrium with the product phase at an equilibrium temperature $T_0$. This temperature corresponds to $\Delta G_c = 0$. For a martensitic transformation, it has been proposed [4] that $T_0 = (A_s + M_s)/2$, where $A_s$ and $M_s$ are the austenitic and martensitic start temperatures respectively. For Nitinol and other alloys that undergo thermoelastic transformation, two equilibrium temperatures were suggested. The first denoted by $T_0$ corresponds to $\Delta G_c = 0$ and is equivalent to $(M_s + A_f)/2$. The other is $T'_0$ where $\Delta G_c + \Delta G_{nc} = 0$ and is equivalent to $(M_f + A_s)/2$ [5]. $A_f$ and $M_f$ are the austenitic and martensitic finish temperatures. For unstressed samples, the ratio of non-chemical free energy, $\Delta G_{nc}$, to the enthalpy of the transformation, $\Delta H_u$, could be estimated using the following formula [6]

$$\Delta G_{nc}/\Delta H_u = (T_0 - T'_0)/T_0 \quad (2)$$

Similarly, the ratio of energy change, $\Delta G$, associated with the cooling of an unstressed sample from $M_s$ to $M_f$, to the change in the entropy of transformation was given as [7]

$$\Delta G_{nc}/\Delta S = (M_f - M_s)/2 \quad (3)$$

where $\Delta S = \Delta H_u/M_s$.

With the DSC, the thermodynamic quantities such as enthalpy, heat capacity, and the temperatures of transformation could be measured. The entropy of

* *Present address*: Department of Mechanical Engineering, University of Saskatchewan, Saskatoon, Saskatchewan, Canada S7N 0W0.



0022–2461 

the reaction is usually calculated from DSC data using the relation $\Delta S = \Delta H_u/T_0$, where $T_0$ is estimated as the average of $A_s$ and $M_s$ [8] or as the average of $A_f$ and $M_s$ when $A_s$ is below $M_s$ [5]. Selected values of these parameters for a near equiatomic Nitinol are given in Table I. It is clear that the values may vary, although the composition of the alloy and its history might be the same. The variation is attributed to the difference in experimental conditions. The sensitivity of the apparatus used is crucial in thermodynamic measurements. The rate of cooling and heating at which transformation occurs also affects the transformation temperatures [9].

Calorimetric studies of the phase transformation of shape memory alloys have been performed with a DSC and have clarified some of the themodynamic characteristics of the parent phase to martensite reaction and vice versa. During the cooling of Nitinol, as the parent phase (B2) transforms into martensite, two exothermic peaks are observed. The sum of enthalpy changes of the two peaks is equal to the enthalpy change of the single endothermic peak occurring with the martensite to B2 phase reaction [16]. Moreover, thermal cycling of Nitinol yields a linear relationship between $\Delta H_u$ and $T_0$, where $T_0 = (A_s + M_s)/2$ [12]. Furthermore, the only study of a surface-constrained shape memory alloy was made on a single crystal of a Cu–Al–Ni alloy. It was found that during the martensitic phase transformation, surface nucleation is inhibited. This results in supercooling to lower temperatures for volume nucleation to take place [17]. Finally, while complete cycling of Nitinol substantially changes the transformation temperatures of the alloy, incomplete cycling does not [18].

In this research, an ultra-low-temperature isotropic (ULTI) carbon, Biolite®, was vapour deposited on the Nitinol substrates. The Biolite® coating is part of a design of prosthesis for the reconstruction of the anterior cruciate ligament [19]. It is the objective of this research work to study the effect of surface coating (constraint) on the phase transformation of Nitinol. The strain energy associated with the surface constraint during the phase transformation is also calculated.

## 2. Materials and methods

Ultra-low-temperature isotropic (ULTI) carbon was vapour deposited on near equiatomic Ni–Ti (50.1 at % Ni–49.9 at % Ti), Nitinol, substrates at Carbomedics, Inc. The vapour-deposition process of the ULTI carbon, Biolite®, is presented elsewhere [20].

Differential scanning calorimetry (DSC) was used to study the effect of surface constraint on the phase transformation of Nitinol. X-ray analysis and Auger electron spectroscopy (AES) were used to study the carbon/Nitinol interface. The procedure followed in preparing samples for these experiments was presented in another publication [19].

Transmission electron microscopy was also used to study the effect of surface constraint on the phase

TABLE I Thermodynamic data of selected Ni–Ti shape-memory alloys

| | Composition (at %) | | | | | | | |
|---|---|---|---|---|---|---|---|---|
| | 49Ni–51Ti | 49.8Ni–50.2Ti | 50Ni–50Ti | 50.1Ni–49.9Ti | 50.4Ni–49.6Ti | 50.5Ni–49.5Ti | 51Ni–49Ti | 55Ni–45Ti |
| Enthalpy of transformation $\Delta H$ (J g$^{-1}$) | 33.05 [10] | 29.04 [11] | 20.08 [10]<br>24.2 [8] | 19.41 [16] | 32.1 [12] | 24.4 [12] | 24.18 [14] | 22.1 [13] |
| Average heat capacity, $C_p$ (J g$^{-1}$ K$^{-1}$) | 0.47 [10] | | 0.47 [8, 10] | 0.58 [16] | | | 0.483 [15] | 0.46 [13] |
| Temperature $T_0$(K) = $(A_s + M_s)/2$ | | 366 [11] | 290 [8]<br>318 [12] | | 308 [12] | 283.6 [12] | | |
| Entropy of transformation $\Delta S$ (J g$^{-1}$ K$^{-1}$) | | 0.079 [11] | 0.101 [12] | | 0.104 [12] | 0.086 [12] | | |
| Reported density (g cm$^{-3}$) | | | 6.4 [8] | | | | 6.45 [15] | |
| Calculated density (g cm$^{-3}$) | 6.48 | 6.49 | 6.49 | 6.49 | 6.50 | 6.50 | 6.50 | 6.56 |

transformation of Nitinol. Because the material under study consisted of a thin carbon film vapour deposited on Nitinol substrates, with TiC at the interface [19], conventional preparation of Nitinol TEM foils was not pursued. Instead, TEM foils made of vertical and horizontal sections of the carbon-coated Nitinol were prepared.

For the preparation of the vertical sections, Nitinol samples, 2.5 mm thick, 4 mm wide, and 20 mm long, were cut using a Buehler Isomet low-speed diamond saw. The samples were wet ground using 600 grit SiC paper, polished with 0.3 μm alumina, and then ultrasonically rinsed in acetone. The samples were vacuum annealed at 550 °C for 1 h, and ULTI carbon was vapour deposited on their surfaces. In order to promote the bond between the carbon and the Nitinol, the carbon-coated samples were heat treated in vacuum at 700 °C for 3 h. Every two samples were glued together along their 20 mm length using super glue. Cross-sections 300 μm thick were then cut using a diamond saw.

The next step involved spark cutting of 3 mm diameter discs of the cross-sections. The diameter of the discs was selected to coincide with the space separating the two carbon-coated surfaces of Nitinol facing each other. The cutting was performed using an Agie electrical discharge machine (EDM) equipped with a 3 mm diameter graphite electrode, and operated at 100 V and 9 A.

Preparation of the TEM foils required reduction of the thicknesses of the cross-sectional samples. After an ultrasonic acetone rinse, the discs were glued to Cu/Rh grids, having 2 mm × 1 mm slits, with super glue. The discs were then wet ground using 600 grit SiC paper to a thickness of 80 μm. The foil thickness was measured using a Gatan precision dimple grinder, model 656. The dimpler was also used to grind the central area of the foil down to 20 μm. Finally, the foils were ion milled from the dimpled side at about 5 kV with a 35 ° gun tilt.

The horizontal sections were easier to prepare than were the vertical sections. Nitinol sheets 0.6 mm thick were annealed at 550 °C for 1 h in vacuum. Biolite® was vapour deposited on only one side of the Nitinol which was then heat treated at 700 °C for 3 h in vacuum. Three mm discs were then spark cut from the carbon-coated plate. The steps that followed were wet grinding the discs from the Nitinol side to a thickness of about 80 μm; dimpling them also from the Nitinol side to 20 μm; and ion milling from the dimpled side at about 5 kV with a 35 ° gun tilt.

Transmission electron microscopy (TEM) was used to examine both foils made of vertical and horizontal sections. The microscope was equipped with a cold stage to study the phase transformation of the surface-constrained Nitinol *in situ*.

## 3. Results

Experimental results of DSC measurements, X-ray analysis and AES were presented in another publication [19]. The major findings were that as the carbon-coated Nitinol samples were heat treated, TiC formed at the interface. Thus, the bond between the Biolite® and Nitinol is enhanced. Also, surface constraint of Nitinol resulted in a marked drop in the $A_s$ and $M_f$ temperatures for thin samples. Fig. 1a and b show the DSC curves in the first cooling cycle for an uncoated Nitinol sample and a 300 nm carbon-coated sample, respectively, that were each heat treated for 3 h at 700 °C. It is shown that although the $M_s$ temperature remains the same for both the coated and uncoated samples, the $M_f$ temperature for the coated and annealed sample dropped markedly in comparison to the uncoated sample. Fig. 2a and b show the DSC curves of the first heating cycle of an uncoated Nitinol sample and a 300 nm carbon-coated sample, respectively, each heat treated for 3 h at 700 °C. It is shown that the $A_f$ temperature for the coated and uncoated samples remains almost the same. However, in case of the coated sample, the $A_s$ temperature dropped significantly in comparison to the uncoated one.

When DSC measurements were made for uncoated and 300 nm carbon-coated samples, annealed at 700 °C for 6 h, similar results were obtained. Fig. 3a and b show the DSC cooling curves of the first cycle for uncoated and coated Nitinol samples, respectively. Fig. 4a and b show the DSC curves for the heating cycle. From both Figs 3 and 4 it is shown that for the constrained samples, the $M_f$ and $A_s$ temperatures dropped markedly, while the $M_s$ and $A_f$ temperatures were almost unchanged.

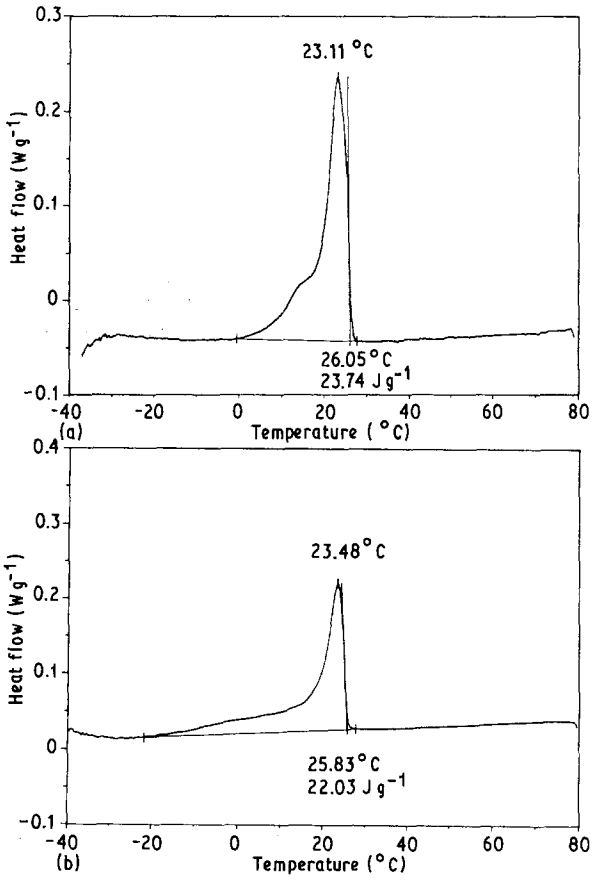


*Figure 1* DSC curves of the first cooling cycle of Nitinol samples, (a) uncoated and annealed at 700 °C for 3 h, (b) coated with a 300 nm, carbon film and annealed at 700 °C for 3 h.

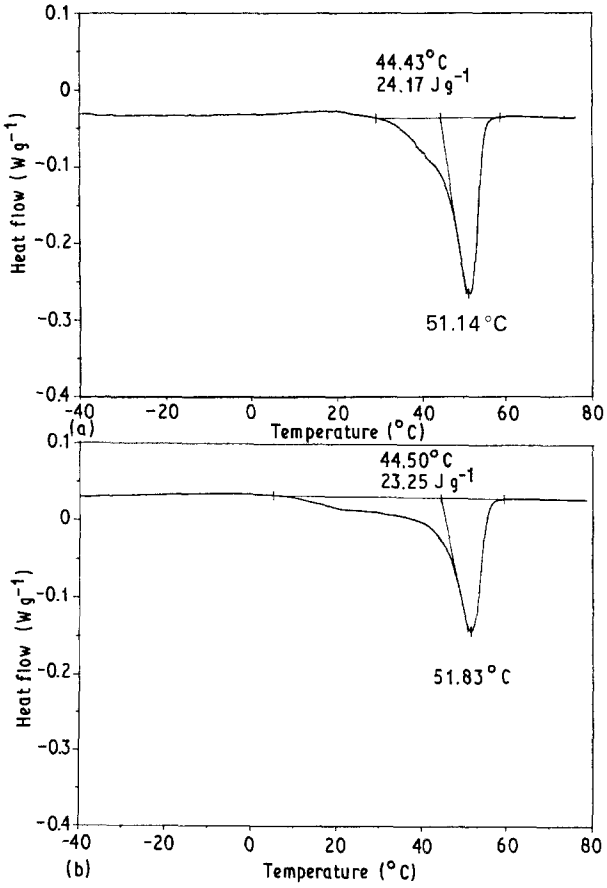


*Figure 2* DSC curves of the first heating cycle of Nitinol samples, (a) uncoated and annealed at 700 °C for 3 h, (b) coated with a 300 nm carbon film and annealed at 700 °C for 3 h.

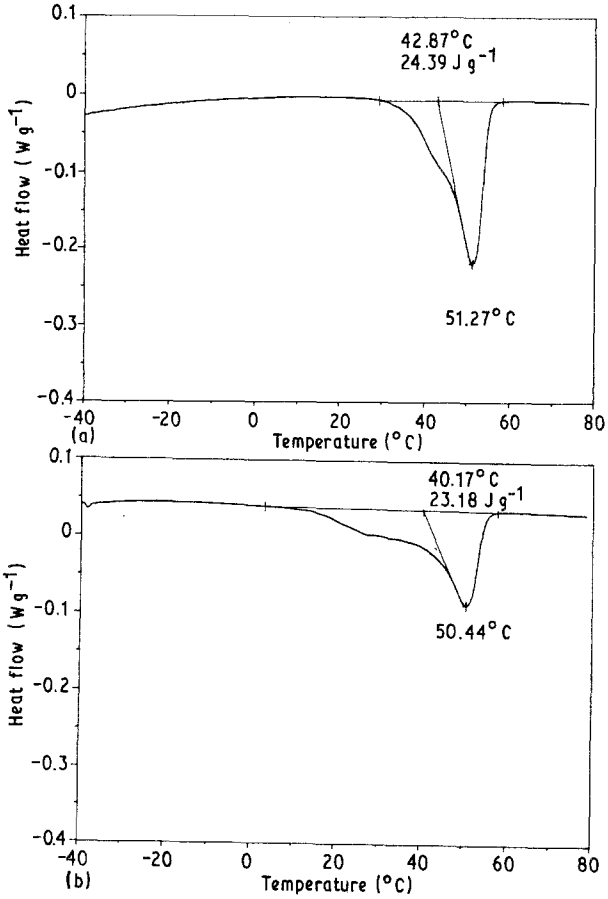


*Figure 4* DSC curves of the first heating cycle of Nitinol samples, (a) uncoated and annealed at 700 °C for 6 h, (b) coated with a 300 nm carbon film and annealed at 700 °C for 6 h.

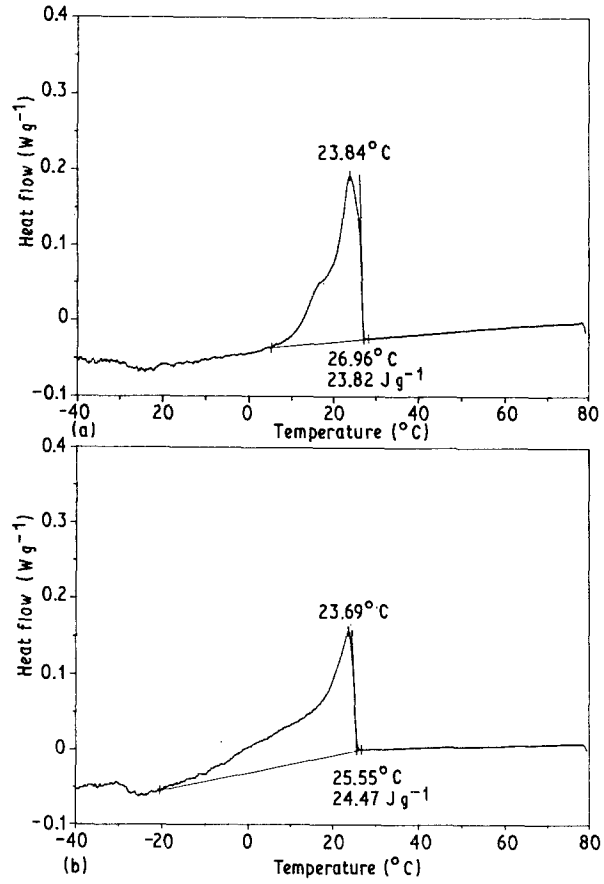


*Figure 3* DSC curves of the first cooling cycle of Nitinol samples, (a) uncoated and annealed at 700 °C for 6 h, (b) coated with a 300 nm carbon film and annealed at 700 °C for 6 h.

TEM foils made of vertical sections of carbon coated Nitinol were examined using transmission electron microscopy. The phase transformation of the surface-constrained Nitinol was studied *in situ* using a cold stage. The TEM foil was cooled below the $M_f$ temperature to ensure complete martensitic transformation of Nitinol. The cooling was then stopped, and the TEM foil was left to warm up in the column to about 300 K. Thus, partial austenitic transformation of the Nitinol occurred. Fig. 5 is a bright-field image of the vertical cross-section TEM foil at about 300 K. The micrograph shows plates of martensite present in the bulk of the Nitinol sample, away from the constrained surface at that temperature. It is proposed that during martensitic transformation, the last martensite to form was close to the constrained surface. Also, the last martensite formed disappeared first in the reverse transformation.

The TiC formed at the carbon/Nitinol interface was investigated with an examination of a horizontal section TEM foil of a 300 nm carbon-coated Nitinol sample heat treated at 700 °C for 3 h. Figs 6 and 7 show the microstructure of TiC and the electron diffraction pattern, $[123]_{TiC}$, corresponding to it, respectively.

## 4. Discussion

The objective of this research work was to study the effect of surface constraint on the phase transformation of Nitinol. The transformation-induced DSC

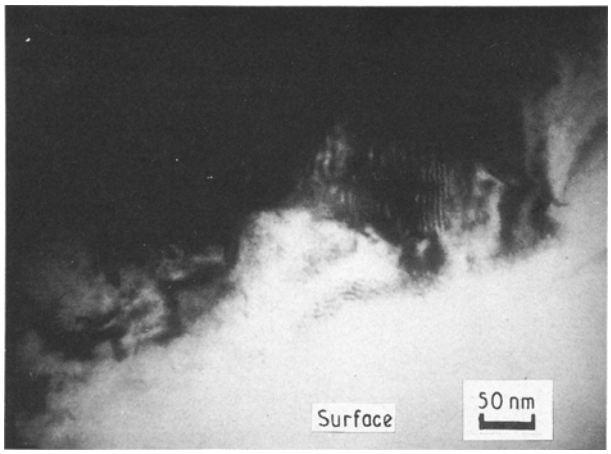


*Figure 5* Bright-field image of a vertical cross-section TEM foil of a 300 nm carbon-coated Nitinol sample heat treated at 700 °C for 3 h.

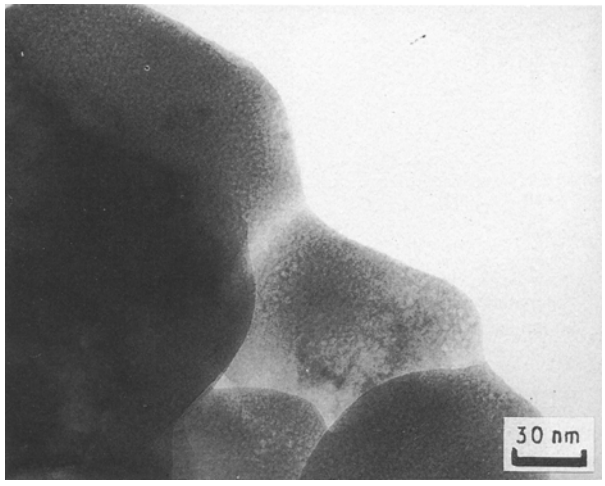


*Figure 6* Bright-field image of TiC.

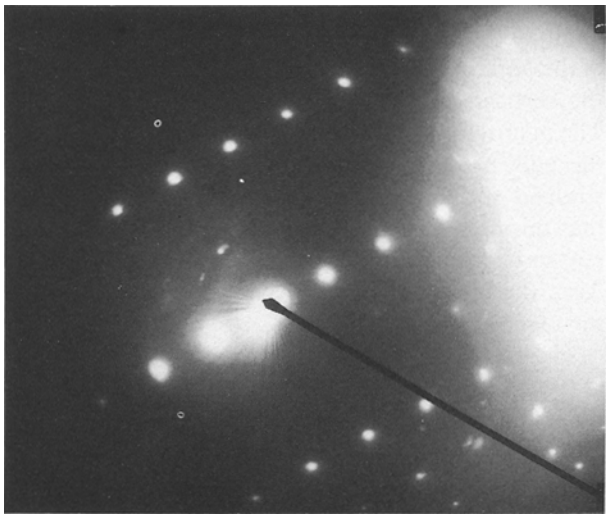

*Figure 7* Electron diffraction pattern of TiC $[123]_{TiC}$.

peaks of the thermally cycled coated and uncoated Nitinol samples were analysed. A DuPont 9900 computer/thermal analyser and the differential scanning calorimeter were used in the analysis. For every thermal peak in the heating or cooling cycle of the Nitinol sample tested, the percentage of the area under the curve as a function of temperature was plotted. The plot also corresponded to the percentage of phase transformed in both the cooling and heating cycles. The analysis with this method was done for the transformation peaks of the coated and uncoated samples on the first cycle of heating and cooling. The analysis was only performed for the coated and uncoated samples that were annealed at 700 °C for 3 and 6 h. Figs 8 and 9 show the effect of surface constraint on the phase transformation of Nitinol for samples annealed at 700 °C for 3 and 6 h, respectively. Both figures represent mapping of the percentage of martensitic phase present in the heating and cooling cycles as a function of temperature. A distinctive characteristic of the figures is how the surface constraint causes the start temperature of the forward reaction and the finish temperature of the reverse transformation to be depressed.

From curve fitting of experimental data, an empirical expression of the following form was obtained for

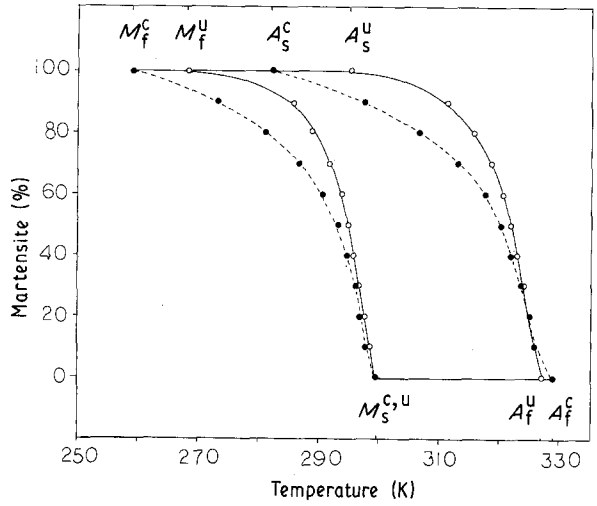


*Figure 8* Per cent martensite as a function of temperature for 300 nm carbon-coated Nitinol samples heat treated at 700 °C for 3 h. (—○—) Uncoated (u), (--●--) coated (c).

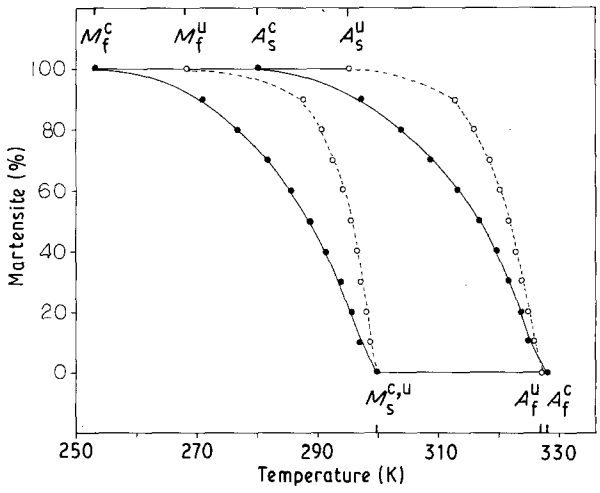


*Figure 9* Per cent martensite as a function of temperature for 300 nm carbon-coated Nitinol samples heat treated at 700 °C for 6 h. (--○--) Uncoated (u), (—●—) coated (c).

the parent to martensite and from martensite to parent phase transformations, respectively.

$$f(A) = \exp[-\alpha(M_s - T)] \quad M_f \leqslant T \leqslant M_s \quad (4a)$$

$$f(A) = \exp[-\gamma(A_f - T)] \quad A_s \leqslant T \leqslant A_f \quad (4b)$$

where $f(A)$ is the fraction of the parent phase (austenite) present at a temperature $T$, and $\alpha$, and $\gamma$ are constants to be evaluated later.

Figure 10a and b represent a comparison of the percentage of the amount of austenitic phase present in uncoated and coated samples, respectively, as a function of temperature during the first cooling cycle. Figs. 10a and b show results of 3 and 6 h annealing, respectively, at 700 °C. Fig. 11a and b represent similar data for the heating cycle. In Figs 10 and 11, solid lines represent the least square fit of experimental data, giving rise to expressions shown in Equation 4a and b.

Equation 4a and b describe, empirically, the fraction of austenite present in the martensitic and reverse transformation, respectively, as a function of temperature. The values of both $\alpha$ and $\gamma$ depended on the testing conditions such as the annealing time, and the presence or absence of surface constraint.

From experimental results, it was found that the curve-fitting constants, $\alpha$ and $\gamma$, for all cases (coated versus uncoated, annealed for 3 or 6 h) could be expressed in terms of the absolute value of the enthalpy of transformation, $\Delta H_u$, and the transformation start

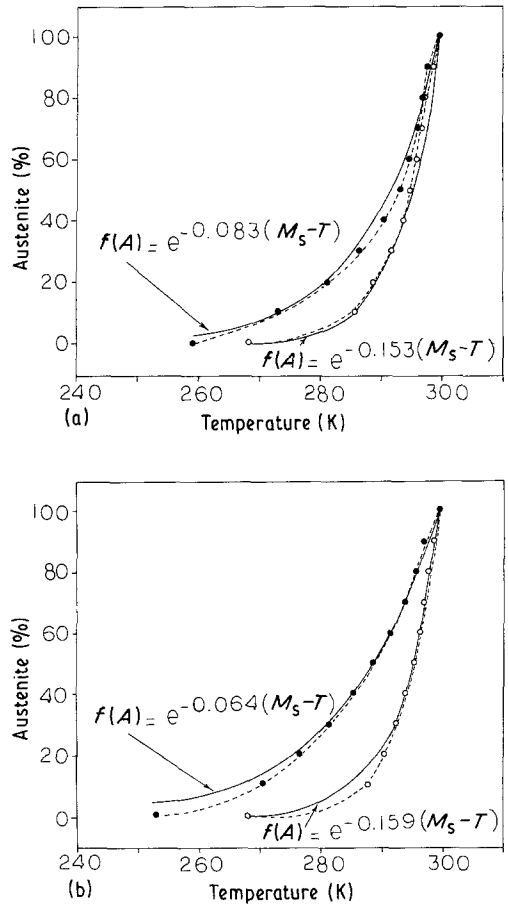


*Figure 10* Per cent austenite present as a function of temperature in the first cooling cycle for (●) coated and (○) uncoated Nitinol samples heat treated at 700 °C for (a) 3 h, (b) 6 h.

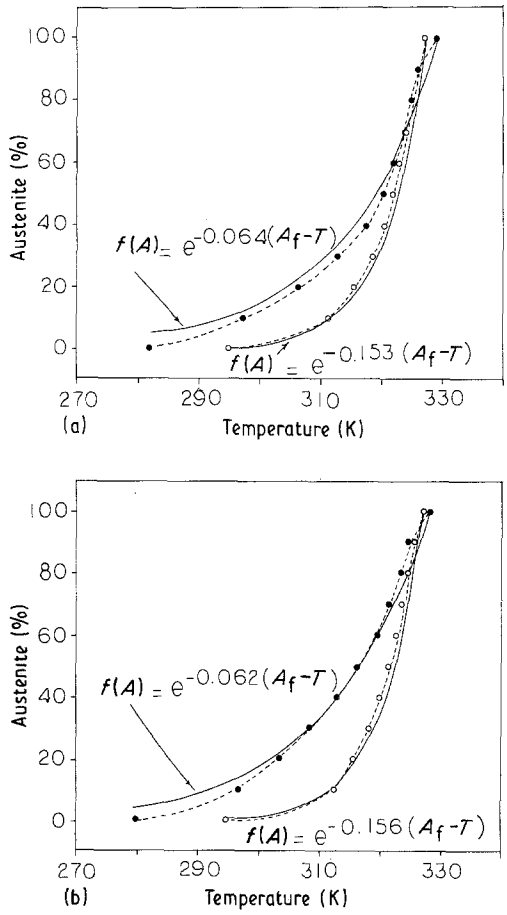


*Figure 11* Per cent austenite present as a function of temperature in the first heating cycle for (●) coated and (○) uncoated Nitinol samples heat treated at 700 °C for (a) 3 h, (b) 6 h.

and finish temperatures

$$\alpha = \Delta H_u / R(M_s - M_f)^2 \quad (5a)$$

$$\gamma = \Delta H_u / R(A_f - A_s)^2 \quad (5b)$$

where $R$ is the gas constant.

Substituting from Equation 5a and b in Equation 4a and b, we have

$$f(A) = \exp - \frac{\Delta H_u(M_s - T)}{R(M_s - M_f)^2} \quad (6a)$$

$$f(A) = \exp - \frac{\Delta H_u(M_s - T)}{R(A_f - A_s)^2} \quad (6b)$$

No chemical compositional change is associated with the martensitic and reverse transformation of Nitinol. Thus, both the parent and the martensitic phase can be treated as a single-component system [21 ]. Fig. 12 is a schematic representation of the molar Gibbs chemical free energy for both the parent phase, $P$, and the martensitic phase, $M$, as a function of temperature. The figure illustrates that there exists a single equilibrium temperature, $T_0$, at which the difference in chemical free energy between the two phases is equal to zero ($\Delta G^{PM} = 0$) [21].

Because of the non-chemical free energies (strain energy and surface energy) associated with the martensitic transformation, it would be expected that the transformation would start at a temperature less than $T_0$. The supercooling below $T_0$ continues until the chemical driving force (chemical free energy decrease)

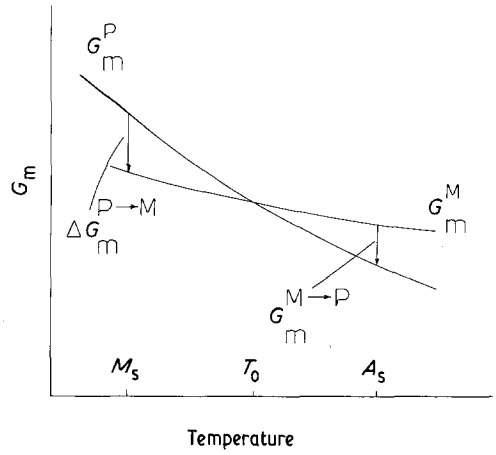


*Figure 12* Schematic representation of $G_m$ as a function of temperature [21].

overcomes the opposing non-chemical energies. The temperature at which this occurs is designated $M_s$. The chemical driving force continues to increase from $M_s$ to $M_f$ at which the transformation is complete [21]. Similarly, in the reverse transformation, superheating above $T_0$ is required. The superheating allows the chemical driving force to overcome the non-chemical energies. Thus, the transformation starts at the $A_s$ temperature and is complete at the $A_f$ temperature.

Equation 6a and b were obtained to express the fraction of the parent phase present as a function of temperature during the martensitic and the reverse transformation, respectively. The cumulative heat of transformation up to a specific temperature, as estimated by the DSC, beyond a transformation start temperature is directly related to the fraction of phase transformed. From the information on fraction transformed, the driving force for the martensitic transformation or the reverse transformation can be calculated.

For the martensitic transformation, it was shown that the fraction of parent phase $f(A)$ present at a specific temperature $M_f \leqslant T \leqslant M_s$ can be represented by Equation 4a. Thus, the fraction of martensite $f(M)$ present at a temperature $M_f \leqslant T \leqslant M_s$ can be represented by $f(M) = 1 - f(A)$, and therefore,

$$f(M) = 1 - \exp[-\alpha(M_s - T)] \quad (7)$$

We assume that the cumulative heat change, $\Delta H$, up to a temperature $T$, as estimated by the DSC, is given by the product of the fraction transformed and the total enthalpy of transformation, $\Delta H_u$. Thus

$$\Delta H = f(M)\Delta H_u \quad (8)$$

From Equations 7 and 8

$$\Delta H = \Delta H_u\{1 - \exp[-\alpha(M_s - T)]\} \quad (9)$$

Using the Gibbs–Helmholtz equation

$$\frac{\partial(\Delta G/T)}{\partial T} = -\frac{\Delta H}{T^2} \quad (10)$$

Thus we can write

$$\frac{\partial(\Delta G/T)}{\partial T} = \Delta H_u\left[\frac{-1}{T^2} + \frac{e^{-\alpha M_s}e^{\alpha T}}{T^2}\right] \quad (11)$$

Upon integration, we can write

$$\left.\frac{\Delta G}{T}\right|_T^{M_s} = \left.\frac{\Delta H_u}{T}\right|_T^{M_s} + \Delta H_u e^{-\alpha M_s}\int_T^{M_s}\frac{e^{\alpha T}}{T^2}dT \quad (12)$$

$$\left.\frac{\Delta G}{T}\right|_{M_s} - \left.\frac{\Delta G}{T}\right|_T = \Delta H_u\left[\frac{1}{M_s} - \frac{1}{T} + e^{-\alpha M_s}\int_T^{M_s}\frac{e^{\alpha T}}{T^2}dT\right] \quad (13)$$

At $T = M_s$, $\Delta G = 0$. Therefore,

$$-\frac{\Delta G}{T} = \Delta H_u\left[\frac{1}{M_s} - \frac{1}{T} + e^{-\alpha M_s}\left(\frac{-e^{\alpha M_s}}{M_s} + \frac{e^{\alpha T}}{T} + \alpha\int_T^{M_s}\frac{e^{\alpha T}}{T}dT\right)\right] \quad (14)$$

$$\Delta G_T = \Delta H_u\left[1 - e^{-\alpha(M_s - T)} - \alpha T e^{-\alpha M_s}\int_T^{M_s}\frac{e^{\alpha T}}{T}dT\right] \quad (15)$$

where the integral $\int_T^{M_s}(e^{\alpha T}/T)dT$ can be calculated with the trapezoid rule of integration. It should be noted that the parent to martensite phase change is an exothermic reaction, and the reverse transformation is endothermic. Therefore, the sign of the enthalpy change must be taken into account.

The calculations of the driving force of the martensite to parent phase transformation, Equation 4b, were used to express the fraction of parent phase $f(A)$ present at a temperature $A_s \leqslant T \leqslant A_f$. Thus, the fraction of martensite $f(M)$ at a temperature $A_s \leqslant T \leqslant A_f$ can be represented by $f(M) = 1 - f(A)$, and therefore,

$$f(M) = 1 - \exp[-\gamma(A_f - T)] \quad (16)$$

Applying Equation 8, we get

$$\Delta H = \Delta H_u\{1 - \exp[-\gamma(A_f - T)]\} \quad (17)$$

Applying the Gibbs–Helmholtz Equation 10 we can write

$$\frac{\partial(\Delta G/T)}{\partial T} = \Delta H_u\left(\frac{-1}{T^2} + \frac{e^{-\gamma A_f}e^{\gamma T}}{T^2}\right) \quad (18)$$

Upon integration, and noting that $\Delta G_T = 0$ at $T = A_s$, the value of $\Delta G$ at the $A_f$ temperature, $\Delta G_{A_f}$, can be estimated. With $\Delta G_{A_f}$ known, $\Delta G_T$ can be calculated from the equation

$$\Delta G_T = \frac{T}{A_f}\Delta G_{A_f} + \Delta H_u\left(1 - e^{-\gamma(A_f - T)} - \gamma T e^{-\gamma A_f}\int_T^{A_f}\frac{e^{\gamma T}}{T}dT\right) \quad (19)$$

where the integral in the right-hand side of Equation 19 can be calculated using the trapezoid rule of integration. Results from Equations 15 and 19 for both coated and uncoated samples are plotted in Figs 13 and 14. In both figures, the solid symbols represent the phase transformation of the coated samples.

The surface constraint was found to affect the driving force. The driving force, $\Delta G$, for the transformation of coated and uncoated samples that were heat

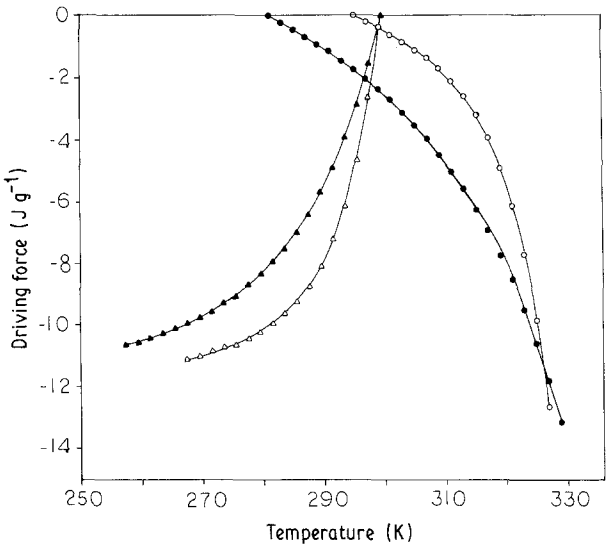


*Figure 13* Driving force as a function of temperature for (○, △) unconstrained and (●, ▲) constrained samples heat treated at 700 °C for 3 h. (●, ○) M → P, (▲, △)P → M.

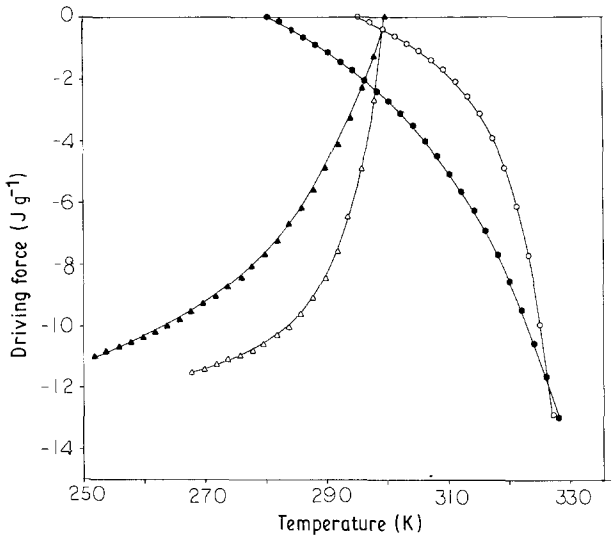


*Figure 14* Driving force as a function of temperature for (○, △) unconstrained and (●, ▲) constrained samples that were heat-treated at 700 °C for 6 h. (●, ○) M → P, (▲, △) P → M.

treated at 700 °C for 3 and 6 h was calculated. Figs 13 and 14 illustrate the driving force as a function of temperature for the unconstrained and constrained Nitinol samples. Both figures show that for the martensitic transformation, $M_s$ is the same for both the constrained and unconstrained sample. However, as the transformation proceeds, the constraint opposes the driving force in the surface-constrained sample. Thus, a more negative value of $\Delta G$, i.e. a larger chemical driving force, is required for further transformation. In order to overcome the constraint and the strain energy associated with it, the constrained sample has to be supercooled to achieve the same driving force required to complete the transformation as in the unconstrained sample. Thus, at any temperature during the martensitic transformation other than $M_s$, the available driving force for the constrained sample is smaller than that for the unconstrained one. From Figs 13 and 14, it appears as though the available driving force associated with complete transformation is less than that for the unconstrained sample. This is due to the fact that complete transformation to martensite in the cooling cycle is never achieved for the constrained sample at the lowest temperature used in these experiments.

In the martensite to parent phase transformation, the $A_s$ temperature for the surface-constrained sample is lower than that of the unconstrained one. This is attributed to the fact that there is an increased amount of strain energy associated with the surface-constrained sample during the martensitic transformation. Release of this stored energy assists in the reverse transformation causing it to start earlier, i.e. at a lower temperature. Thus, the driving force is greater in the constrained sample in the reverse transformation as compared to the unconstrained one at any temperature during the reverse transformation. Because the accommodation strain is largest for the martensite plates formed near the constrained surface, the reverse transformation of the surface-constrained sample starts at or near the surface and proceeds to the bulk with the increase in temperature.

Finally, the strain energy associated with the surface constraint of the Nitinol samples could be estimated. Figs 13 and 14 show the differences in the driving force between the unconstrained and constrained samples at a given temperature during martensitic and reverse transformations. This difference corresponds to the strain energy contributed by the surface constraint, and is a function of temperature. It is significant to point out that the strain energy associated with surface constraint depends on the ratio of volume of surface constraint to that of the bulk. Thus, for thin samples, where the volume of the constraining surface layer is a significant fraction of the bulk, the elastic stored energy can have a measureable effect on the transformation behaviour. This is in contrast to samples with a small volume of constraining surface layer compared to that of the bulk. In the latter case, the elastic stored energy will have a negligible effect on the transformation behaviour.

## Acknowledgements

The authors thank Dr Axel Haubold and Mr Al Beavan, Carbomedics, Inc., for coating the Nitinol substrates used in this research work with Biolite®. The authors also acknowledge funding of this work through Michigan State Research Excellence Fund (REF) administered through the Composite Materials and Structures Center of Michigan State University.

## References

1. K. MUKHERJEE, in "Encyclopedia of Materials Science and Engineering", edited by Michael Bever (Pergamon Press, New York, 1986), p. 4368.
2. J. PERKINS, *ibid.* p. 4365.
3. C. WAYMAN, in "Physical Metallurgy", edited by R. Cahn and P. Haaser (North-Holland Physics, Amsterdam, 1983) p. 1031.

4. L. KAUFMAN and M. COHEN, in "Progress in Metal Physics", vol. 7, edited by B. Chalmers and R. King (Pergamon Press, New York, 1958), p. 165.
5. H. TONG and C. WAYMAN, *Acta. Metall.* **22** (1974) 887.
6. *Idem., ibid.* **23** (1975) 209.
7. M. AHLERS, R. PASCUAL and R. RAPACIOLI, *Mater. Sci. Engng* **27** (1977) 49.
8. O. MERCIER and K. MELTON, *J. Appl. Phys.* **52** (1981) 1030.
9. J. KWARCIAK and H. MORAWIEC *J. Mater. Sci.* **23** (1988) 551.
10. O. MERCIER and K. MELTON, *J. Appl. Phys.* **50** (1979) 5747.
11. R. WASILEWSKI, S. BUTLER and J. HANLON, *Metal Sci. J.* **1**(7) (1967) 104.
12. G. AIROLDI, B. RIVOLTA and C. TURCO, in Proceedings of the International Conference on Martensitic Transformations (ICOMAT-86), Nara, Japan 26–30 August 1986, edited by the Japan Institute of Metals.
13. R. SALZBRENNER, *J. Mater. Sci.* **19** (1984) 1827.
14. F. WANG, W. BUEHLER and S. PICKART, *J. Appl. Phys.* **36** (1965) 3232.
15. F. WANG, B. DESAVAGE and W. BUEHLER, *ibid.* **39** (1968) 2166.
16. K. MUKHERJEE, S. SIRCAR and N. DAHOTRE, *Mater. Sci. Engng* **74** (1985) 75.
17. R. SALZBRENNER and M. COHEN, *Acta. Metall.* **27** (1979) 739.
18. T. TADAKI, Y. NAKATA and K. SHIMIZU, *Trans. Jpn. Inst. Metals* **28** (1987) 883.
19. A. HEDAYAT, J. RECHTIEN and K. MUKHERJEE, *J. Mater. Sci. Mater. Med.* **3** (1992) 65.
20. A. HAUBOLD, in "Encyclopedia of Materials Science and Engineering", edited by Michael Beuer (Pergamon Press, New York, 1986) p. 514.
21. K. MUKHERJEE, in "International Summer Course on Martensitic Transformations (ICOMAT-82)", Leuven, Belgium, edited by Katholieke Universiteit Leuven (6–7 August, 1982).

*Received 13 June*
*and accepted 31 October 1991*